The Use of Piezoelectric Ceramics for Electric Power Generation Within Orthopedic Implants

Article *in* IEEE/ASME Transactions on Mechatronics · September 2005

DOI: 10.1109/TMECH.2005.852482 · Source: IEEE Xplore

4 authors, including:

Shane Farritor
University of Nebraska at Lincoln
154 PUBLICATIONS **2,938** CITATIONS

SEE PROFILE

Hani Haider
University of Nebraska Medical Center
300 PUBLICATIONS **2,714** CITATIONS

SEE PROFILE

Short Papers

The Use of Piezoelectric Ceramics for Electric Power Generation Within Orthopedic Implants

Stephen R. Platt, Shane Farritor, Kevin Garvin, and Hani Haider

***Abstract*—This paper presents the results of tests that demonstrate the feasibility of using piezoelectric (PZT) ceramics to generate *in vivo* electrical energy for orthopedic implants. Sensors encapsulated within implants could provide *in vivo* diagnostic capabilities such as the monitoring of implant duty (i.e., walking) cycle, detecting abnormally asymmetric or high forces, sensing misalignment and early loosening, and early detection of wear. Early diagnosis of abnormalities or impending failure is critical to minimize patient harm. However, the routine use of sensors and microprocessors embedded within orthopedic implants for diagnostic and monitoring purposes has been limited by the lack of a long-term self-contained power source capable of lasting the expected 20-year implant lifetimes.**

By embedding PZT materials within orthopedic implants, a small amount of the mechanical energy generated during normal physical activity can be converted into useful electrical energy. This *in vivo* energy source can power embedded microprocessors and sensors for a broad range of biomedical uses. The current work investigates the application of this technology to total knee replacement (TKR) implants, but it is applicable to many other implanted biomedical devices.

***Index Terms*—Orthopedics, piezoelectric (PZT) ceramics, piezoelectric (PZT) materials, power generation.**

I. Introduction

More than 250 000 total knee replacement (TKR) [1] and 180 000 total hip replacement (THR) [2] operations are conducted in the United States each year. Approximately 71% of the knee and 58% of the hip replacement surgeries are performed on patients over age 65 [3]. This age group is expected to increase to more than 100 million individuals during the next 75 years [4]–[6]. The growth of this demographic group is expected to be accompanied by a similar growth in joint replacements.

Although TKR implants have an expected lifetime of up to 20 years, there are many premature failures. The most frequent cause of failure is excessive wear of the ultrahigh molecular weight polyethylene material used in most designs to provide a low friction bearing surface [7]. Reactions to the resulting polyethylene particulate debris often lead to joint swelling (synovitis) or bone degradation (osteolysis) [8]. Wear can also lead to misalignment or instability of the joint, changing implant kinematics and damaging other implant components [9]. Also, surgical misalignment can accelerate wear and wear-induced loosening by causing asymmetric loads [2].

Implant failure requires revision surgery that is generally more complex and traumatic than first-time knee replacement. Such surgeries account for over 8% of all TKR operations [10]–[12]. Early detection of excessive implant wear and/or incipient failure is essential if these procedures are to be avoided, and would help lower medical costs and reduce trauma.

Self-powered embedded implant sensors could provide new *in vivo* diagnostic capabilities that reduce these clinical complications. Instrumented implants could process measurements, store results, and communicate them noninvasively to the attending surgeon or therapist. Integrated sensors could monitor the implant duty cycle (i.e., walking), detect component wear, sense changes in alignment, log abnormal forces, and detect loosening. These measurements could extend the lifespan and improve the function of implants. However, the lack of a long-term power source currently restricts the use of embedded sensors to short-term laboratory studies. Within the physical constraints of TKR implants, current batteries cannot meet the expected lifetime power requirements [13] for a continuous diagnostic and monitoring system. This paper presents a new approach for providing long-term self-contained *in vivo* power.

Manuscript received September 23, 2003; revised April 5, 2004. Recommended by Technical Editor I.-M. Chen. This work was supported by the Christina M. Hixon Fund.

S. R. Platt, S. Farritor, and K. Garvin are with the Department of Mechanical Engineering, University of Nebraska-Lincoln, Lincoln, NE 68588-0656 USA (e-mail: srp@unlserve.unl.edu; sfarritor@unl.edu; kgarvin@unmc.edu).

H. Haider is with the Department of Orthopedic Surgery, University of Nebraska Medical Center, Omaha, NE 68198-1080 USA (e-mail: hhaider@unmc.edu).

Digital Object Identifier 10.1109/TMECH.2005.852482

II. Related Research

A. Sensors in Orthopedic Implants

The use of sensors in orthopedic implants has generally been limited to laboratory settings due in part to cumbersome and bulky power sources and the concomitant limitations imposed by not having a truly unobtrusive data acquisition system. Previous research studies have incorporated sensors in both hip and knee implants to measure joint forces and implant environmental conditions. These systems either had a finite lifespan (batteries) or received power from large external equipment (induction). One study used temporary implants that contained four load cells to quantify knee joint forces [14], and a second study measured tibial forces [15]. Other research has measured loads in distal femoral replacements [16]–[18], forces and temperatures in hip implants [19], [20], and deflections of implants [21]–[23].

All of the above work used magnetic induction or leads passing through the skin to provide power from an external source. The systems were designed to log data only for short periods of time. The patients were tethered to external equipment for power and data transmission, significantly limiting the range and type of activities that could be studied.

The goal of this work is to help enable the routine use of self-powered sensors in clinical implants. This work specifically addresses the problem of providing electrical power for an integrated, autonomous, and long-term diagnostic and monitoring system that can be widely used for both research and therapeutic purposes.

B. PZT Power Generation

Mechanical deformation of a piezoelectric (PZT) element distorts an internal dipole moment and creates a voltage. This material can therefore be used as a generator that converts the mechanical energy of compression into electrical energy. Activities such as walking transmit a large amount of mechanical power through the hip and knee joints relative to the needs of microelectronic systems. It has been estimated that 67 W is generated in the heel/ground interaction of an average human walking at a rate of two steps per second [24]. The axial force across a TKR implant during normal walking can reach three times body weight several times per step [25]. Some of this mechanical energy could be used to compress a PZT element and produce electrical power.

PZT materials have been extensively studied as actuators and sensors [26], [27], however, their use as electrical generators is less established. The practical challenges of developing a PZT generator for low-frequency (e.g., 1-Hz walking rate) operation include poor source characteristics, such as high-voltage, low-current, high-capacitive impedance, and relatively low-power output [28]–[30].

Previous studies have demonstrated or proposed the use of PZT materials to extract electrical energy from a variety of mechanical energy sources. These sources include walking [30], [31], machine and building vibrations [32], [33], water flow in oceans and rivers [29], the kinetic energy of explosive projectiles on impact [34], and pressure variations in micro-hydraulic systems [35]. Potential medical applications include the use of PZT materials to generate electricity to promote bone growth [36] and attaching PZT strips to the rib cage or aorta of a patient to provide power for a cardiac pacemaker [37]–[41].

The above studies have all had some success in extracting a small amount of electrical power from PZT elements. However, many issues such as efficiency and power conditioning and storage have not been fully addressed. These studies also do not address the size, power, shape, material, and implementation constraints of biomechanical implant systems. For example, many of the above studies have used relatively flexible PZT films or specially manufactured PZT ceramics that allow for high deflections and high strains. Such large deflections (e.g., $>$6–10 mm) are not acceptable in TKR implants because of the important kinematic relationships that must be maintained. Therefore, the results of prior research cannot be directly applied to this work. The current work presents the first demonstration of using PZT elements to generate useful electrical power within orthopedic implants.

III. Simulations and Experiments

A. Experimental Design

1) A Self-Powered TKR Implant Model: A conceptual model of self-powered instrumented implants is illustrated in Fig. 1. Fig. 1(a) shows a tibial tray of the shape typically used in TKR applications that has been redesigned by making it deeper and including three stems to accommodate three PZT elements (also shown). Body force is applied by the femoral component to the bearing surface and a distribution plate is used to transfer the load to the three elements.

Three PZT elements are used to provide a stable support for the load distribution plate. Each rectangular ($1.0 \times 1.0 \times 2.0$ cm) element is constructed as a stack of multiple (≈ 145) PZT layers, each with a pair of electrodes (Piezo Systems^{TM}). The layers are mechanically in series (equal stress) and are electrically connected in parallel. The elements are approximately located so an axial force is evenly distributed in each element. The primary purpose of the PZT elements is to convert mechanical input power into electrical power. Because the output of the PZT elements is proportional to the input axial force, it is in principle also possible to use these same elements as axial force sensors. PZT load cells and force sensors are widely available. However, in an actual implant, the forces will be multi-axis and the contact points between the femoral component and the bearing will move. The electrical design described in Section IV-B will accommodate unequal forces, and if excessive deflection occurs, the load distribution plate will contact the tibial tray limiting further motion. It is these anterior—posterior shear forces that are the primary causes of wear in TKR implants. Therefore, it is anticipated that an actual instrumented implant will incorporate specially designed sensors distinct from the PZT elements to monitor precisely the forces and wear experienced within the implant. Such a sensor could take many forms, but could be as simple as a stray-field capacitor measuring the thickness of the bearing surface.

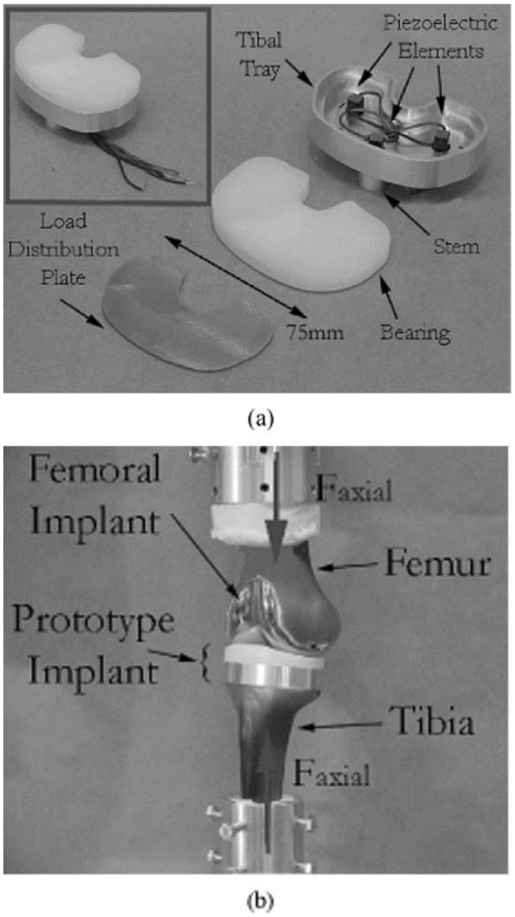

Fig. 1. (a) Self-powered TKR model and test setup. Components of the implant model. (b) Test setup.

Fig. 1(b) shows the implant model mounted on an anatomically correct synthetic tibia and femur (Sawbones^{TM}). The two bones are cemented into jigs that are attached to a single-axis Mini-Bionix MTS machine that is used to apply the axial force profiles.

These figures are graphic illustrations of some of the physical constraints within which any power generation and biosensing system must fit. The modification of a fixed bearing implant design to enclose PZT elements and the associated conditioning and sensor electronics is only one of many possible concepts. The current work is not intended to address the complex details of implant design. Many additional implant design constraints must be considered before clinical implementation is possible. For example, the current design incorporates a polyethylene bearing surface that slides vertically within the tibial tray. The total displacements are small (<10 μm) and may not significantly increase the degree of wear in implants (e.g., Walker, 2000). However, alternative approaches are possible. For example, the edges of the insert could be fixed (e.g., molded) to the tibial tray, eliminating the sliding motion and associated frictional forces. Mechanical forces could then be transmitted to the PZT elements by allowing center deflection of an appropriately designed bearing surface, much like the surface of a drum. This approach would also address the need to seal the electronics to avoid fluid seepage. Encapsulating electrical components, whether in sealed compartments or using any of a variety of coatings (e.g., epoxy), is a common technique used to protect the components from environmental conditions and this will be explored in the future. The

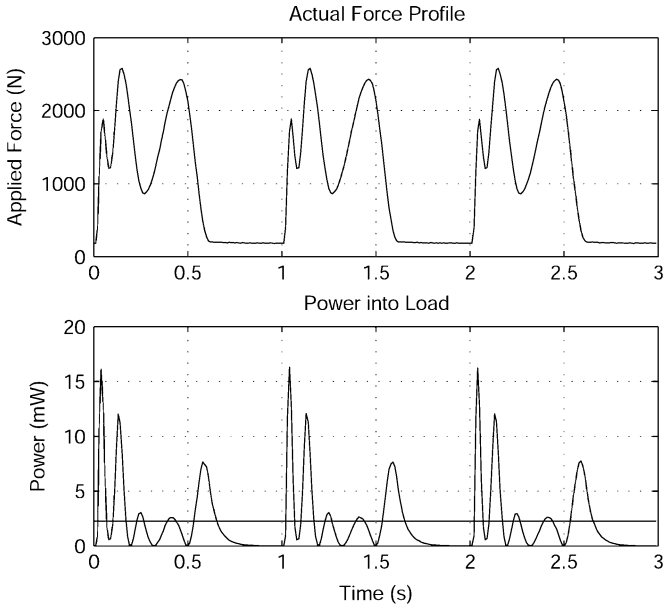

Fig. 2. Time history of input axial force and dissipated power.

goal of the current work with this very simple physical model is to show that PZT power generation is feasible within the volume, force, and deflection constraints of TKR implants. The following sections summarize the results of this work.

2) MTS 858, Data Acquisition, and Input Force Waveforms: Laboratory tests were performed to quantify the electrical power that could be generated. The specimens were subjected to various cyclic mechanical loads on a single-axis Mini-Bionix MTS 858 test machine. This machine is equipped with a Proportional-Integral-Derivative (PID) controller and is capable of applying arbitrary force or displacement waveforms to the PZT samples. Forces are measured using a calibrated load cell, and displacements are measured using an onboard linear variable displacement transducer (LVDT).

A PC running a custom Labview application communicating to a 12-bit National Instruments 6025E PCI DAQ card was used to generate force waveforms and to record all force, displacement, and voltage measurements. All measurements were made under steady state conditions, at a rate of 400 samples/s, and for a duration of approximately thirty seconds each. Within each data file, corresponding samples for each applied force cycle were averaged together to reduce noise. Average values for power and root-mean-square (rms) voltage were calculated by integrating across all samples and weighting appropriately for the sample rate and frequency of the applied force for values of load resistors ranging from 1 kΩ to 1 MΩ.

Tests were conducted using low-frequency (1–10 Hz) sinusoidal input force waveforms with amplitudes ranging from 400 to 3000 N and the International Standards Organization (ISO) force waveform for the typical axial forces found in TKR implants [Fig. 2(top)] [42]. This force has several peaks that reach 2–3 times body weight during the load bearing stance phase and drops to near zero during the swing phase of the ($\approx$1 Hz) walking cycle.

B. Electrical Power Generation and Conditioning

Experiments were performed to determine the raw power dissipated in resistive loads (R_L) by subjecting the PZT elements to cyclic force profiles. The instantaneous power dissipated in the load is given by $(V_{\rm out}^2/R_L)$, where $V_{\rm out}$ is the voltage measured across the load. A typical result under the ISO force profile is shown in Fig. 2. The top plot shows three cycles of the input force waveform, and the bottom plot shows the instantaneous and average power (horizontal line) delivered to the resistive load.

A series of these measurements were made for a range of resistive loads. For each resistive load, the time series data were integrated and a value for the average power delivered to the load was calculated. The maximum average power produced by a single PZT stack under a 900 N amplitude ISO knee force profile is approximately 1.6 mW into a matched resistive load. This implies that three such elements, as in the conceptual TKR model, would produce 4.8 mW of continuous raw power under expected force loading conditions.

This result suggests that sufficient raw power is available under realistic TKR forces to operate current generation low power microprocessors and sensors. As can be seen in the time-series plot of Fig. 2, however, the output from this generator is characterized by very high ripple. The transient nature and relatively high-voltage output from this generator is clearly not appropriate for low-power digital electronics without significant signal conditioning.

To demonstrate the feasibility of a self-powered TKR implant, the simple application circuit shown in Fig. 3 was developed. The raw bipolar PZT output is first converted to a unipolar signal using full-bridge rectifiers. A 10-μF capacitor is used to smooth the PZT output signal and to store excess energy during each force cycle. The 2.6 V output of a low power linear regulator (Maxim MAX 666) is used to power a PIC 16LF872 microprocessor. This low power processor has digital I/O, multiple analog input lines, non-volatile memory, and an onboard 10-bit analog to digital converter. The processor has the capabilities to perform many of the basic monitoring and diagnostic tasks for the instrumented implants envisioned in this work.

Transforming the raw power from the PZT elements into useful regulated power is not straightforward. At low frequencies these elements are essentially capacitive devices [43], [44]. The use of a capacitor to smooth and store the raw PZT output amounts to transferring energy directly between capacitors—an inherently inefficient process.

The optimal value of this storage capacitor depends upon the source impedance of the PZT generator, the total load of the circuit components, and the amount of ripple that can be tolerated by the application. Fig. 4 shows simulation and laboratory results for the total power delivered by the three PZT stacks per ISO knee force cycle for a wide range of storage capacitors and resistive loads. Two representative plots (inset) show results for cross-sections of constant resistance ($R_L = 9.76$ kΩ) and constant storage capacitance ($C_s = 10$ μF), and each data point represents a laboratory experiment. The simulation results were calculated using a lumped element electromechanical model for the PZT element [28], [45].

For low values of the storage capacitor, the maximum power delivered to a matched load approaches 4.8 mW, the expected value based on the initial raw power measurements. Voltage drops and losses in the rectifiers account for the slightly lower results obtained here. As expected, small values of C_s reduce the system to a rectified version of the raw power experiment. At the same time, a small C_s will have little effect on the level of output ripple.

Increasing the value of the storage capacitor reduces the amount of ripple but also reduces the energy transfer efficiency. Fig. 4 (bottom right), shows that adding a 10-μF capacitor reduces the efficiency of this circuit to about 40% compared to the total raw power delivered by three PZT elements to a purely resistive load. This operating point was chosen as a compromise between maximizing energy transfer efficiency and minimizing output ripple.

Fig. 5 shows the regulated voltage (middle) and microprocessor (bottom) output of the test circuit for the applied ISO axial force profile (top) using a 10-μF storage capacitor. The microprocessor was

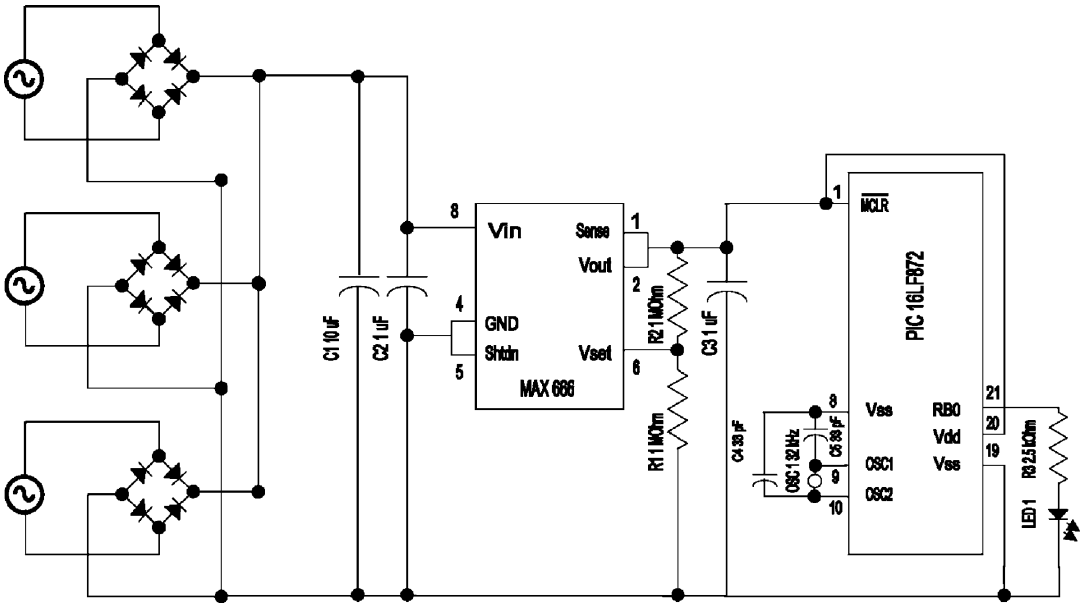

Fig. 3. Electrical design.

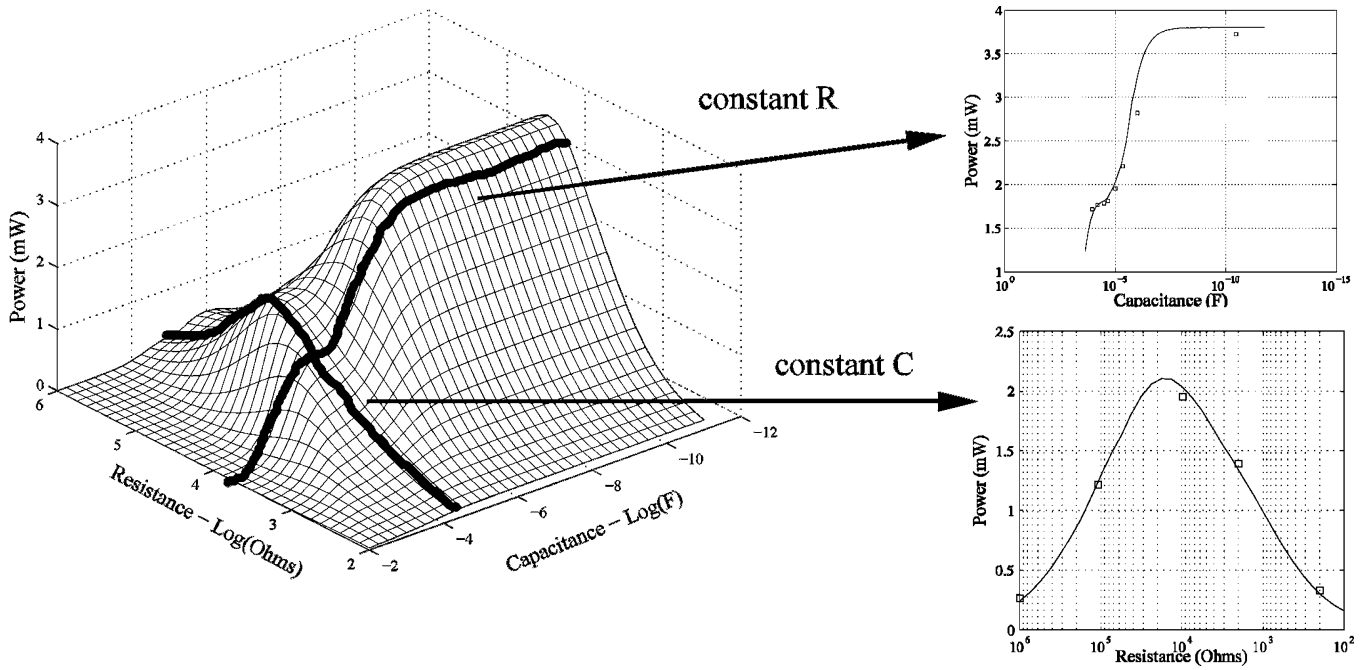

Fig. 4. Power generated versus R_L and C_S.

programmed to turn an LED on for a fixed period during each force cycle. This system delivers approximately 850 μW (327 μA at 2.6 V) of continuous regulated power. Overall electrical efficiency is approximately 19%. Further experiments showed that sufficient power is generated to continuously operate the microprocessor even with the amplitude of the applied force reduced by 50%.

The power generated by the current prototype is not sufficient to operate continuously currently available low-power data transmission systems (e.g., Bluetooth). However, there are a variety of alternative approaches that could be used for transmitting the acquired data. For example, Kymissis *et al*. [30] demonstrated a shoe-insert PZT generator that operated a low-power RF radio transmitter in a burst mode. By storing excess power either in a battery or capacitor, similar approaches could be used in the current work. Alternatively, all data could be stored in nonvolatile memory for later downloading in a setting where external sources of power (e.g., inductive coupling) could

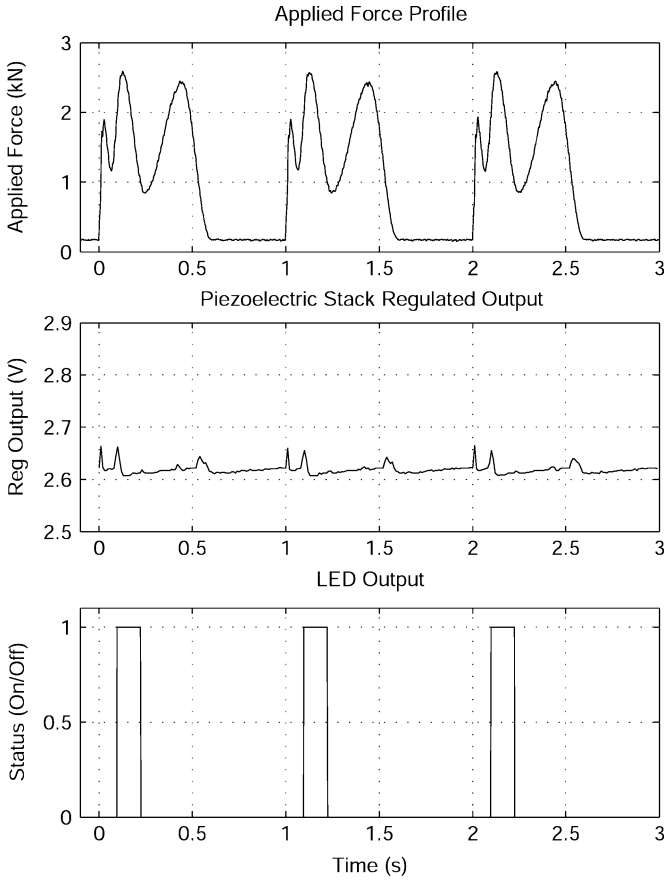

Fig. 5. Regulated power output and microprocessor output.

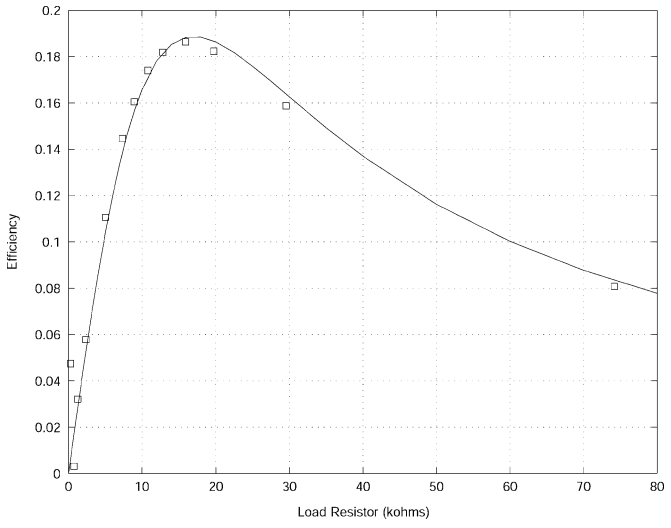

Fig. 6. Electromechanical efficiency at 1 Hz.

be used to power the data transmission system. The details of the data transmission system will depend significantly on the specific requirements of each application.

C. Electromechanical Efficiency

The efficiency with which input mechanical power is converted to raw electrical power by the PZT elements used in this work is shown in Fig. 6. The squares show the measured efficiency of conversion as a function of load resistor for a 1-Hz input force profile, and the solid line shows the predicted result using a PZT electromechanical model [28]. The input mechanical power is calculated directly from the measured values of the input force and PZT displacement. The raw electrical power delivered to the load is calculated by measuring the voltage across the load resistor.

These results indicate that overall electromechanical conversion efficiency is approximately 20% for a load that matches the PZT source impedance. The efficiency decreases rapidly for mismatched loads, illustrating the importance of matching source and load characteristics.

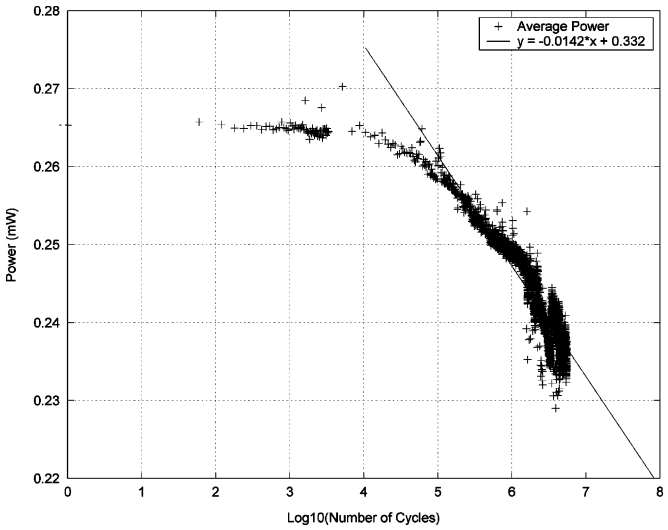

Fig. 7. Longevity.

D. Longevity

It is well known that repeated mechanical and electrical cycling of PZT ceramics results in a progressive degradation in performance as a function of time [46]–[48]. The actual degradation depends on application specific details such as the amplitude, frequency, and duration of the applied electrical and mechanical loads, as well as the composition of the PZT material [49], [50].

A PZT implant generator must function efficiently for 20–40 million cycles. No data currently exist on the performance characteristics of PZT ceramics subject to the conditions expected within TKR implants. To characterize the long-term performance of a PZT TKR generator, the raw electrical power delivered to a matched resistive load by a single PZT stack was monitored for approximately six million cycles of a 440-N amplitude ISO knee force profile. The amplitude of the input force was chosen to be the same as the load that would be experienced by each of the three elements of the triple stack combination under 50% of full load. The average power delivered to the resistive load is shown in Fig. 7.

Beyond negligible degradation in electrical output during the first 10^4 cycles, the output decreases approximately linearly per decade of time. This test was interrupted several times by unexpected shutdowns of the MTS hydraulic test machine. These shutdowns, the worst of which occurred at 1.6 million cycles, caused very high transient ($\sim$15 KN) hydraulic hammer impulse forces. Impulses of this type are known to cause a semi-permanent drop in performance of PZT elements [51]. Upon restarting the test, the electrical output continues to decay in a logarithmic fashion, albeit usually at a lower level compared to pre-shutdown conditions. The PZT element also displays some recovery in electrical output that correlates with an increase in the length

of time between the shutdown event and restarting the test. This effect has been seen in other studies of cyclic loading of PZT ceramics [52], although the mechanism driving the recovery is not well understood.

The best fit straight line shown superimposed on the data spans the range of $10^4 - 1.6 \times 10^6$ cycles. No attempt was made to correct for changes in output due to test machine shutdown events. Even this conservative approach predicts a drop in the electrical output of less than 17% of the initial value after 20 million cycles. Thus, this PZT generator appears able to produce useful electrical power for tens of millions of cycles at the low frequencies and loads expected for a TKR application.

IV. Summary and Conclusions

This paper presents results that suggest PZT ceramics can be used to generate sufficient electrical energy within TKR implants to operate low power microprocessors and sensors for diagnostic and monitoring applications. A major limitation to widespread, clinical use of embedded implant sensors is the lack of a long-term self-contained power supply. By encapsulating PZT materials within orthopedic implants, a small amount of the mechanical energy generated during normal physical activities can be converted into useful electrical energy.

The results indicate that three PZT ceramic elements with a total volume of 1.2 cm^3 embedded within a TKR implant can generate 4.8 mW of raw electrical power under expected axial loading conditions. A simple, prototype power conditioning circuit was used to transform the raw PZT output into regulated electrical power which was used to continuously operate a low-power microprocessor. Laboratory measurements show that the efficiency of transforming mechanical input power into raw electrical power is approximately 19%, in excellent agreement with the electromechanical model and simulation tools developed during this work. The overall efficiency of converting input mechanical power into useful electrical energy is approximately 4% with the prototype conditioning circuit. Time degradation of the electrical output of the PZT elements used in this work after 6.5 million cycles under expected TKR loading conditions indicate deterioration of less than 17% over the expected 20-year lifetime of an implant.

Future work will include the development of more efficient power conditioning circuitry that addresses the capacitive nature and other poor source characteristics of PZT generators. An initial suite of sensors and a more detailed implant design are also required. The application of this technology to hip replacement implants will also be investigated.

Acknowledgment

The experimental work was performed at the Biomechanics Lab. in the Department of Orthopedic Surgery at the University of Nebraska Medical Center, September 23, 2003.

References

[1] S. Mendenhall, Editorial, *Orthopaedic Network News*, vol. 11, no. 1, Jan. 2000, p. 7.

[2] T. M. Wright and S. B. Goodman, eds., "Implant wear in total joint replacement: Clinical and biological issues, material and design considerations," Rosemont, IL, *Amer. Acad. Orthoped. Surg.*, p. 3, Oct. 2001.

[3] Advance Data No. 329 [Online]. Available: http://www.cdc.gov/nchs/fastats/pdf/ad329t8.pdf/, 2002. CDC-Centers for Disease Control and Prevention.

[4] Total Population by Age, Race and Hispanic or Latino Origin for the United States [Online]. Available: http://www.census.gov/prod/cen2000/docs/sf1.pdf, 2000. United States Census Bureau, Census 2000 Summary File 1.

[5] Projections of the Total Resident Population by 5-Year Age Groups, and Sex With Special Age Categories: Middle Series, 2025 to 2045 [Online]. Available: http://www.census.gov/ population/projections/nation/summary/np-t3-f.pdf, 2000. United States Census Bureau.

[6] Projections of the Total Resident Population by 5-Year Age Groups, and Sex With Special Age Categories: Middle Series, 2050 to 2075 [Online]. Available: http://www.census.gov/ population/projections/nation/summary/np-t3-g.pdf, 2000. United States Census Bureau.

[7] J. P. Collier *et al.*, "Analysis of the failure of 122 polyethylene inserts from uncemented tibial knee components," *Clin. Orthopaed. Rel. Res.*, vol. 273, pp. 232–242, Dec. 1991.

[8] T. P. Schmalzried and J. J. Callaghan, "Current concepts review: wear in total hip and knee replacements," *J. Bone Joint Surg. A*, vol. 81, no. 1, pp. 115–136, Jan. 1999.

[9] P. S. Walker *et al.*, "Methodology for long-term wear testing of total knee replacements," *Clin. Orthopaed. Rel. Res.*, vol. 372, pp. 290–301, Mar. 2000.

[10] B. Espehaug, O. Fumes, L. I. Havelin, L. B. Engasaeter, and S. E. Vollset, "The type of cement and failure of total hip replacements," *J. Bone Joint Surg. B*, vol. 84, no. 6, pp. 832–838, Aug. 2002.

[11] O. Furnes, B. Espehaug, S. A. Lie, S. E. Vollset, L. B. Engesaeter, and L. I. Havelin, "Early failures among 7174 primary total knee replacements: A follow-up study from the Norwegian arthroplasty register 1994–2000," *Acta Orthopaed. Scand.*, vol. 73, no. 2, pp. 117–129, Apr. 2002.

[12] M. A. Ritter, "Direct compression molded polyethylene for total hip and knee replacements," *Clin. Orthopaed. Rel. Res.*, vol. 393, pp. 94–100, Dec. 2001.

[13] S. R. Platt "Electric Power Generation Within Orthopaedic Implants Using Piezoelectric Ceramics," M.S. Thesis, Dept. Mechanical Eng., Univ. Nebraska-Lincoln, Lincoln, NE, 2003.

[14] B. A. Morris, D. D. D'Lima, J. Slamin, N. Kovacevic, N. S. W. Arms, C. P. Townsend, and C. W. Colwell Jr., "e-Knee: Evolution of the electronic knee prosthesis," *J. Bone Joint Surg.*, vol. 83-A, Suppl 2 (pt 1), pp. 62–66, Oct. 2001.

[15] K. R. Kaufman, N. Kovacevic, S. E. Irby, and C. W. Colwell, "Instrumented implant for measuring tibiofemoral forces," *J. Biomech.*, vol. 29, no. 5, pp. 667–671, May 1996.

[16] E. Schneider, M. C. Michel, M. Genge, K. Zuber, R. Ganz, and S. M. Perren, "Loads acting in an intramedullary nail during fracture healing in the human femur," *J. Biomech.*, vol. 34, no. 7, pp. 849–857, Jul. 2001.

[17] S. J. G. Taylor and P. S. Walker, "Forces and moments telemetered from two distal femoral replacements during various activities," *J. Biomech.*, vol. 34, no. 7, pp. 839–848, Jul. 2001.

[18] S. J. G. Taylor, P. S. Walker, J. S. Perry, S. R. Cannon, and R. Woledge, "The forces in the distal femur and the knee during walking and other activities measured by telemetry," *J. Arthroplasty*, vol. 13, no. 4, pp. 428–437, Jun. 1998.

[19] F. Graichen, G. Bergmann, and A. Rohlmann, "Hip endoprosthesis for *in vivo* measurement of joint force and temperature," *J. Biomech.*, vol. 32, no. 10, pp. 1113–1117, Oct. 1999.

[20] D. T. Davy, G. M. Kotzar, R. H. Brown, K. G. Heiple, V. M. Goldberg, K. G. Heiple Jr., J. Berilla, and A. H. Burstein, "Telemetric force measurements across the hip after total arthroplasty," *J. Bone Joint Surg.*, vol. 70, no. 1, pp. 45–50, Jan. 1988.

[21] D. G. Mendes, G. Barak, and E. Mendes, "IntelliJoint system for monitoring displacement in biologic systems," *IMAJ*, vol. 4, no. 1, pp. 69–70, Jan. 2002.

[22] F. Burny, M. Donkerwolcke, F. Moulart, R. Bourgois, R.. Puers, K. Van Schuylenbergh, M. Barbosa, O. Paiva, F. Rodes, J. B. Begueret, and P. Lawes, "Concept, design and fabrication of smart orthopedic implants," *Med. Eng. Phys.*, vol. 22, no. 7, pp. 469–479, Sep. 2000.

[23] A. Ishikawa, N. Takeda, S. I. Ahn, S. S. Ahn, S. R. Hays, and F. A. Gaffney, US patent 6447448 Miniature Implanted Orthopedic Sensors, Sep. 2002.

[24] T. Starner, "Human powered wearable computing," *IBM Syst. J.*, vol. 35, no. 3–4, pp. 618–629, 1996.

[25] J. B. Morrison, "The mechanics of the knee joint in relation to normal walking," *J. Biomech.*, vol. 3, no. 1, pp. 51–61, Jan. 1970.

[26] G. Gautschi, *Piezoelectric Sensorics*. New York: Springer Verlag, 2001.

[27] K. Uchino, *Piezoelectric Actuators and Ultrasonic Motors*. Boston, MA: Kluwer Academic, 1996.

[28] "On low-frequency electric power generation with PZT ceramics," *IEEE Trans. Mech.*, vol. 10, Apr. 2005, pp. 240–252.

[29] G. W. Taylor, J. R. Burns, S. M. Kamman, W. B. Powers, and T. R. Welsh, "The energy harvesting eel: A small subsurface ocean/river power generator," *IEEE J. Ocean. Eng.*, vol. 26, no. 4, pp. 539–547, Oct. 2001.

[30] J. Kymissis, C. Kendall, J. Paradiso, J. , and N. Gershenfeld, "Parasitic power harvesting in shoes," presented at the 2nd IEEE Int. Conf. Wearable

Computing (MIT Media Laboratory), pp. 132–139, Los Alamitos, CA: IEEE Computer Society Press, Aug. 1998.
[31] N. S. Shenck and J. A. Paradiso, "Energy scavenging with shoe-mounted piezoelectrics," *IEEE Micro*, vol. 21, no. 3, pp. 30–42, May 2001.
[32] P. Glynne-Jones, S. P. Beeby, and N. M. White, "Towards a piezoelectric vibration-powered microgenerator," *IEEE Sci. Meas. Technol.*, vol. 148, no. 2, pp. 68–72, Mar. 2001.
[33] S. Roundy, "The power of good vibrations," *Lab Notes-Research From the College of Engineering*, vol. 2, no. 1, Berkeley, CA: Berkeley Press, Jan. 2002.
[34] T. G. Engel, "Energy conversion and high power pulse production using miniature piezoelectric compressors," *IEEE Trans. Plasma Sci.*, vol. 28, no. 5, pp. 1338–1340, Oct. 2000.
[35] N. W. Haggod IV *et al.*, "Development of micro-hydraulic transducer technology," presented at the 10th Int. Conf. on Adaptive Structures and Technologies, Paris, France, Oct. 1999.
[36] C. S. McDowell, "Implanted Bone Stimulator and Prosthesis System and Method of Enhancing Bone Growth," U.S. Pat. 6 143 035, Nov. 7, 2000.
[37] C. C. Enger and J. H. Kennedy, "Piezoelectric power sources utilizing the mechanical energy of the human heart," presented at the 16th Annual Conf. Engineering in Medicine and Biology, Baltimore, MD, Nov. 1963.
[38] ——, "An improved bioelectric generator," *Trans. Am. Soc. Artif. Intern. Organs*, vol. 10, pp. 373–377, Oct. 1964.
[39] W. H. Ko, "Piezoelectric energy converter for electronic implants," presented at the 19th Annual Conf. Engineering in Medicine and Biology, San Francisco, CA, Nov. 1966.
[40] G. H. Meyers *et al.*, "Biologically energized cardiac pacemakers," *IEEE Trans. Bio-Med. Eng.*, vol. BME-10, p. 83, Apr. 1963.
[41] G. H. Meyers *et al.*, "Biologically energized cardiac pacemakers," *Amer. J. Med. Electron.*, vol. 3, pp. 233–236, Oct/Dec. 1964.
[42] ISO 14243-1:2002(E) Implants for surgery-wear of total knee-joint prostheses—Part 1: Loading and displacement parameters for wear-testing machines with load control and corresponding environmental conditions for test. Int. Org. for Standardization, 03, 2002.
[43] V. E. Bottom, *Introduction to Quartz Crystal Unit Design*. New York: Van Nostrand Reinhold, 1982.
[44] W. G. Cady, *Piezoelectricity: An Introduction to the Theory and Applications of Electromechanical Pheonomena in Crystals*. New York: Dover, 1964, vol. 1 & 2.
[45] M. Rossi, *Acoustics and Electroacoustics*. Norwood, MA: Artech House, 1988.
[46] "Effects of high static stress on the piezoelectric properties of transducer materials," vol. 33, no. 10, pp. 1339–1344, Oct. 1961.
[47] M. D. Hill, G. S. White, and C. Hwang, "Cyclic damage in lead zirconate titanate," *J. Amer. Ceram. Soc.*, vol. 79, no. 7, pp. 1915–1920, Jul. 1996.
[48] M. G. Cain, M. Stewart, and M. G. Gee, "Degradation of Piezoelectric Materials," National Physical Laboratory Management Ltd., Teddington, Middlesex, U.K., TW11 0LW, NPL Rep. SMMT (A) 148, 1999.
[49] G. Yang, S. F. Liu, W. Ren, and B. K. Mukherjee, "Uniaxial stress dependence of the piezoelectric properties of lead zirconate titanate ceramics," "in *Active Materials: Behavior and Mechanics*," SPIE Proceedings Bellingham, WA, vol. 3992, pp. 103–113, 2000.
[50] "Domain processes in lead zirconate and barium titanate ceramics," vol. 30, no. 11, pp. 1804–1810, Nov. 1959.
[51] F. Lowrie, M. Cain, and M. Stewart, "Time dependent behaviour of piezoelectric materials," National Physical Lab. Management Ltd., Teddington, U.K., TW11 0LW, NPL Rep. SMMT (A) 151, 1999.
[52] D. M. Breiner "Deterioration of soft PZT due to cyclic loading," M.S. thesis, Univ. of Nebraska-Lincoln, 1997.

Denoising Jet Engine Gas Path Measurements Using Nonlinear Filters

Rajeev Verma and Ranjan Ganguli

***Abstract*—Traditionally, linear filters have been used to smooth time series of gas path measurements before performing fault detection and isolation. However, linear filters can smooth out sharp trend shifts in the signal and are also not good at removing outliers. Since most fault detection and isolation algorithms are optimized for Gaussian noise, they can show performance degradation when outliers are present. In this study, numerical results with simulated data for engine deterioration and abrupt fault show that the nonlinear rational filter with median preprocessor are useful for gas turbine health monitoring applications resulting in noise reduction of 73%–96% while preserving signal features and removing outliers.**

***Index Terms*—Fault diagnosis, gas turbines, signal processing.**

I. Introduction

Health monitoring applications typically involve detection and isolation of a system fault based on a comparison between a "good" baseline system and a "damaged" system [1]. A health signal can be interpreted as a measurement delta between the damaged measurement $z^{(d)}$ and undamaged measurement $z^{(u)}$ and written as $\Delta = z^{(d)} - z^{(u)}$. Under ideal conditions, when a system has no fault, $\Delta = 0$. When a fault occurs, Δ assumes a nonzero value whose magnitude depends of the size and location on the fault. In this idealized system, the nonzero value of the measurement deviation, along with other measurement deviations, can be used to detect and isolate the fault.

Studies of gas turbine data have shown two main features of the health signal Δ: 1) most major problems in the engine are caused by a "single fault" which is preceded by a sharp trend shift [2] and 2) long-term deterioration in the engine causes a low-order polynomial variation in the measurements with time, with a linear polynomial being a very good approximation [3]. However, noise and outliers are present in the gas turbine health signals. Therefore, processing of health signals is often done before using fault isolation methods using linear filters [4]. However, linear filters smooth out the sharp edges in the signal that contain important information about the fault initiation time as well as repair events and could be used for fault isolation applications. Furthermore, linear filters are not good at removing outliers in the data. For commercial aircraft engines, only few data points are received for each flight. Therefore, it is important to keep the forward data point requirement to a minimum. In this paper, we explore nonlinear rational and median filters with a low-time delay for gas turbine applications.

II. Gas Turbine Diagnostics

Fig. 1 shows a schematic of a turbofan engine which has five modules: fan, low-pressure compressor (LPC), high-pressure compressor (HPC), low-pressure turbine (LPT), and high-pressure turbine (HPT). Faults in the gas turbine engine cause efficiency deterioration for the engine modules. The engine state is monitored using at least the four basic sensors: exhaust gas temperature (EGT), fuel flow (WF), low rotor speed (N1), and high rotor speed (N2). The measurement deltas ΔEGT, ΔWF, ΔN1, and ΔN2 are used for estimating the engine

Manuscript received March 18, 2003; revised July 9, 2003. Recommended by Technical Editor J. van Amerongen.

R. Verma is with the Advanced Engineering, Ashok Leyland Ltd., Chennai 600035, India (e-mail: rajeevverma.alc@ashokleyland.com).

R. Ganguli is with the Department of Aerospace Engineering, Indian Institute of Science, Bangalore 560012, India (e-mail: ganguli@ aero.iisc.ernet.in).

Digital Object Identifier 10.1109/TMECH.2005.852454